Remaining Useful Life Prediction With Deep Learning Methods

(Final report)

Thomas Guillebot de Nerville*, Paul Strähle*, Anass Akrim†‡ and Rob Vingerhoeds†

*Institut Supérieur de l'Aéronautique et de l'Espace (ISAE-SUPAERO), Université de Toulouse, 31400 Toulouse, FRANCE
Email: {thomas.guillebot-de-nerville,paul.strahle}@student.isae-supaero.fr

†Institut Supérieur de l'Aéronautique et de l'Espace (ISAE-SUPAERO), Université de Toulouse, 31400 Toulouse, FRANCE
Email: {anass.akrim,rob.vingerhoeds}@isae-supaero.fr

‡Institut Clément Ader (UMR CNRS 5312) INSA/UPS/ISAE/Mines Albi, Université de Toulouse, 31400 Toulouse, FRANCE
Email: anass.akrim@univ-tlse3.fr

Abstract—With the increasing availability of data for Prognostics and Health Management (PHM) data driven approaches become more and more interesting. Deep Learning is one of these approaches. As Deep Learning has shown great success in other domains such as Natural Language Processing (NLP) and image classification it is a promising prospect for PHM.

This paper aims to compare Deep Learning models to predict the Remaining Useful Life (RUL) of a structure. The investigated models are the following: the Convolutional Neural Network (CNN) family with the 1D-CNN and Temporal Convolutional Network (TCN) architectures and the Recurrent Neural Network (RNN) family with the RNN, Long short-term memorys (LSTMs) and Gated Recurrent Units (GRUs) architectures.

The dataset for training and testing consists in simulations of the crack growth in plates, based on the Paris-Erdogan law. The training and validation dataset is composed of 10 000 structures while the testing dataset is composed of 100 structures. Each architecture is optimized and trained on respectively 100, 500 and 1000 structures from the training dataset. At the end, the different models are evaluated and compared on the testing dataset on the basis of the accuracy metric.

Both the GRU and TCN models show a validation accuracy of greater than 95% when trained on 500 or 1000 structures. But the TCN outperforms all other models on the testing dataset where it reaches 100% accuracy after being trained on 1000 structures.

All results of this study as well as the created code is available publicly at https://github.com/blitzpaal/RUL-Prediction.

I. BACKGROUND

A. Deep Learning

In recent years Deep Learning, a subbranch of Machine Learning, has shown impressive results, especially in the fields of speech recognition, visual object recognition and object detection [1]. One requirement in using Deep Learning is the presence of sufficient amounts of data [2]. As more data becomes available in the engineering domain there is a recent surge of interest in using Deep Learning in engineering [3].

One of the strengths of Deep Learning approaches is their ability to deal with and detect complex relationships in large datasets [4]. This strength makes their usage also interesting in the PHM domain [5]. The potential of Deep Learning in PHM might not be fully exploited yet [6].

B. Prognostics and Health Management

According to Zio [7] PHM is a field of research and application which aims at making use of past, present and future information on the environmental, operational and usage conditions of a piece of equipment in order to detect its degradation, diagnose its faults, predict and proactively manage its failures. In the context of this project only the detection of degradation and prediction of failure are relevant.

PHM models can be divided into single and multi-model approaches. Multi-model approaches are a combination of different single-model approaches. Single-model approaches can be further divided into knowledge-based, data-driven and physics-based models. Within the data-driven models there are statistical, stochastic and Machine Learning models which is the category of Deep Learning models. [4]

II. INTEREST

Deep Learning has shown some impressive results when applied to RUL prediction as shown in [8]–[13] and other publications (For an overview see Akrim et al. [6]).

Within the available Deep Learning models there are two algorithms which are promising for RUL prediction: RNNs (Little [14] and Hopfield [15]) and CNNs (Lecun et al. [16]) [6].

RNNs are the common Deep Learning approach for time-dependent relationships and have therefore also achieved great interest in the PHM domain [6]. Pioneering models were developed such as Elman Recurrent Networks (ERMs) [17] or Jordan Networks [18], outperforming traditional Multilayer Perceptrons (MLPs) for sequence-prediction [6]. These algorithms were then widely explored by several researchers. Among them can be cited Yan et al. [19] for their work on material degradation evaluation and life prediction in 2007, and Kramti et al. [20] for having used ERMs for high-speed shaft bearing prognostics based on vibration signals [6].

An emerging type of Deep Learning network for time-dependent relationships are CNNs which might be able to outperform RNNs [21]. In one of the first applications of CNNs to PHM Li et al. suggested that CNNs can be used

to obtain RUL prognoses for machinery [9]. The model was applied to the C-MAPSS dataset [22] and outperformed state-of-the-art prognostics approaches including RNN and LSTM models.

In this work a synthetic dataset is used as according to Fink et al. [23] the use of simulation environments and adaption to real-life applications is a promising future research approach as the data will more likely be sufficient in the source domain. The synthetic dataset used for this study aims at using this advantage.

The synthetic dataset matches strain gauge data to RUL values. The use of strain gauges as an input to a PHM model is interesting as they play a vital role in PHM in general [24] and specifically for the aircraft domain [25].

III. AIM

The aim of this study is to predict the RUL of precracked plates based on strain gauge measurements using Deep Learning. For the application of Deep Learning to crack growth for RUL prediction based on strain gauge measurements no relevant results in the literature could be found. This study attempts to fill this research gap.

In our work the Paris-Erdogan Law [27] was used to create a synthetic dataset of crack growth to train the model. The dataset consists of strain data from virtual strain gauges placed in the area around the crack and the corresponding RUL of the plates.

The Paris-Erdogan Law is applied to an infinite plate with a central horizontal crack. The strain gauges are placed in a 45°-Angle at the positions shown in Figure 1 relative to the center of the plate where the crack is located.
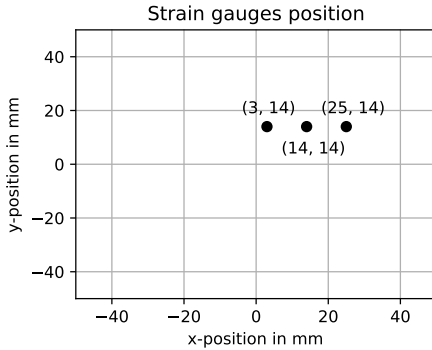

Fig. 1. Position of the strain gauges relative to the crack

The crack length in the Paris-Erdogan Law is a function of the number of cylces k, stress range $\Delta\sigma$, material constants m, C and initial crack length a_0. By calculating the crack growth until the crack length a reaches the critical crack length $a_{crit} = \left(\frac{K_{IC}}{\Delta\sigma\sqrt{\pi}}\right)^2$ the simulation can determine the RUL for each simulated cycle. For the simulations the stress range $\Delta\sigma$ is kept constant while the initial crack length a_0 and the material parameters m and C are drawn from a normal distribution. $10\,000$ structures are generated this way to form the training and validation datasets. For the testing dataset 100

structures are generated. The output of these simulations which forms the input and output for the Deep Learning models is a table matching the strains from the strain gauges to the RUL. To reduce the dataset the results are only saved to the table every 500 cycles. Table I shows the structure of the generated training and validation dataset. The label ID denotes the specific structure.

TABLE I
TRAINING AND VALIDATION DATASET STRUCTURE

t	ID	$cycle$	ϵ_1	ϵ_2	ϵ_3	RUL
1	1	0	$\epsilon_{1,1}$	$\epsilon_{2,1}$	$\epsilon_{3,1}$	RUL_1
2	1	500	$\epsilon_{1,2}$	$\epsilon_{2,2}$	$\epsilon_{3,2}$	RUL_2
3	1	1000	$\epsilon_{1,3}$	$\epsilon_{2,3}$	$\epsilon_{3,3}$	RUL_3
4	1	1500	$\epsilon_{1,4}$	$\epsilon_{2,4}$	$\epsilon_{3,4}$	RUL_4
$\vdots$	$\vdots$	$\vdots$	$\vdots$	$\vdots$	$\vdots$	$\vdots$
n	$10\,000$	$N_{f,10\,000}$	$\epsilon_{1,n}$	$\epsilon_{2,n}$	$\epsilon_{3,n}$	RUL_n

The aim of this work is to predict the RUL based on current and past information from the 3 strain gauges time series using Deep Learning models. Different Deep Learning model architectures are to be used for that. The developed models should be trained and optimized before a comparison between them is made.

IV. METHODS

A. Available Dataset

The created training and validation dataset with $10\,000$ structures is divided into different subsets for training and validation. The last 100 structures of the training dataset are always used as the validation dataset. For training either the first 100, 500 or 1000 structures are used. One training run with the TCN architecture is performed using $9\,900$ structures for training and therefore using the full dataset for training and validation. For testing the models always the same testing dataset with 100 structures is used.

As it showed promising results in other applications of Deep Learning to PHM ([28], [29]), classification is an interesting alternative to regression for RUL prediction. Instead of trying to predict an exact RUL value the goal is to predict the correct RUL class with a lower and upper bound for the RUL. The structures in the generated dataset have a RUL value of around $80\,000$ cycles at most. Therefore the chosen strategy is to create 19 intervals following a parabolic equation between 0 and $80\,000$ cycles. Figure 2 shows the principal output of the neural networks as well as the boundaries between the RUL classes. After the 19 classes following the parabolic equation a last class is added for all RUL values greater than $80\,000$ cycles. The total number of classes is therefore $C = 20$. The reason to use the parabolic equation for class generation is to generate more classes near a RUL value near 0 as it is more critical to generate accurate predictions near the failure of the structures.

To prepare the data as an input and output for the networks a sliding window approach is used. This approach maps the RUL at time t onto the current and past time steps of the input
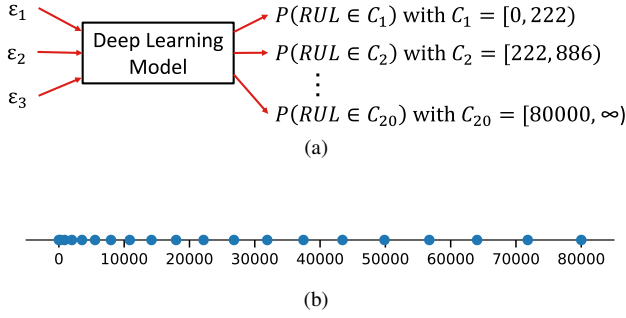
(a)

(b)

Fig. 2. (a): Neural network model output for RUL classification, (b): Boundaries between the RUL classes (The dots represent the boundaries)

features $[x_{t-N+1}, x_{t-N+2}, ..., x_{t-1}, x_t]$ where N is the length of the sliding window. The resulting input matrix therefore has the dimension $(n - N) \times N \times k$ where n is the number of samples and k is the number of features. Figure 3 shows an example of how the time series data of the strain gauges from Table I is mapped to the input matrix.
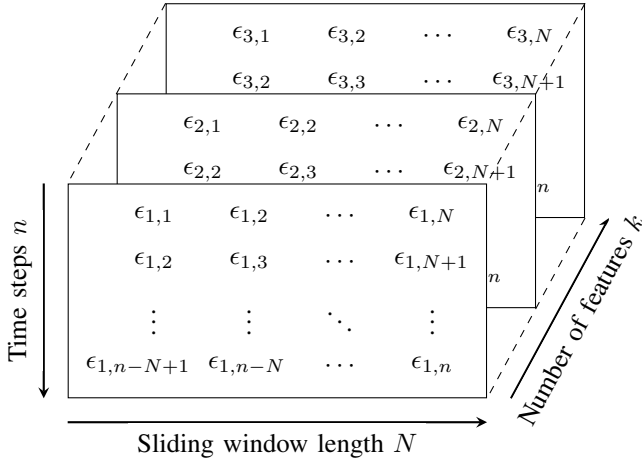

Fig. 3. Input matrix for the neural networks

The output matrix shown in Figure 4 is only one dimensional. It is only composed of the RUL classes which are mapped to the corresponding rows in the input matrix. The dimension of the output matrix therefore is $(n - N)$.
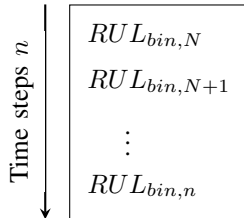

Fig. 4. Output matrix for the neural networks

As an input for the different models, the datasets are normalized. While a specific layer is added at the beginning of the 1D-CNN architecture to do so, the preprocessed data

has to be normalized before being fed into the different RNN models.

B. Recurrent Neural Networks

The common type of Deep Learning model for time series prediction are RNNs [21]. Due to their ability to store information within the cell, it can better remember information of time-dependent data.
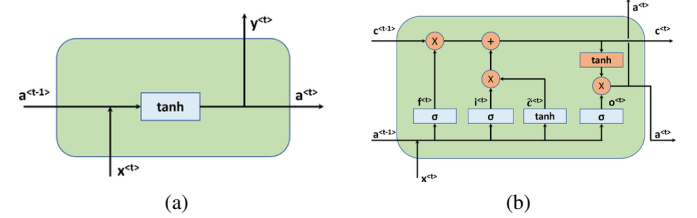

Fig. 5. Different RNN cell architectures: (a): Simple RNN unit, (b): LSTM unit [30]

However, standard RNNs have some major drawbacks, such as the vanishing or exploding gradient problem, which limit their application [31]. LSTM networks (Hochreiter and Schmidhuber [32]) avoid this problem and have established themselves as one of the most used Deep Learning model type, especially for NLP [33]. For these reasons LSTMs will be one of the investigated RNN approaches in this project. Another investigated RNN approach is the GRU. It is a simplified version of the LSTM. Due to this simplicity it has been gaining in popularity in recent years [34].

The key idea to GRUs and LSTMs is the memory cell which allows the network to remember information without much loss.

The LSTM architecture consists of an input gate, a forget gate and an output gate. The input gate decides to add new information from the present input to the present cell state scaled by how much it wishes to add them. The forget gate allows the cell to know how to partially forget the previous cell state. Then, the output gate decides what to output from the new cell state.

For the GRU architecture, only two gates are implemented. The update gate decides the portion of updated candidate needed to calculate the current cell state, which in turn also decides the portion of the previous cell state retained. The relevance gate calculates how relevant the previous information is, and then is used in the candidate for the updated value.

A simple RNN architecture will also be explored to evaluate the possible benefits of more complex architectures such as LSTMs and GRUs. A RNN unit only has a tanh layer after combining the cell state and the candidate.

C. Convolutional Neural Networks

Recent results suggest that CNNs can match or even outperform RNNs in time series related tasks [21]. The second major network type of this work are therefore CNNs.

The common CNN models deal with 2-Dimensional data as input such as pictures. The time sequence data used for PHM

is in 1-Dimensional format. For this application 1D-CNN have been introduced. The key differences between them and the 2D-CNNs are that their input data is reduced by one dimension and that the convolution filter only slides in one direction [6]. Figure 6 shows an example of a simple 1D-CNN architecture with an illustration of the filter sliding over the time series.
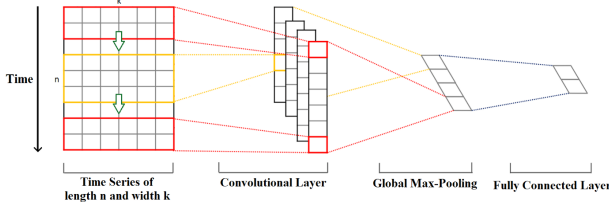

Fig. 6. Example of a 1D-CNN architecture [35]

Besides the 1D-CNN architecture TCNs (Bai et al. [21]) are investigated in this work. A TCN is a specific CNN architecture that tries to replicate some of the best practices for CNN architectures. As depicted in Fig. 7 a TCN is composed of multiple layers which include dilation. The dilation for each layer can be set arbitrarily but it is common practice to use multiples of 2 for it. Through dilation TCNs can increase their receptive field and therefore capture relationships over longer time sequences. One TCN layer is composed of a TCN residual block (see Figure 8 (a)). One block consists of two dilated convolutional layers. The activation function for the layers is usually the ReLU function. The residual blocks include dropout and normalization layers between the convolutional layers. The blocks also include an optional skip connection with a 1x1 convolutional layer. Figure 8 (b) shows an exemplary TCN block with a kernel size of $k = 3$ and a dilation of $d = 1$. For more details on TCNs see [21].
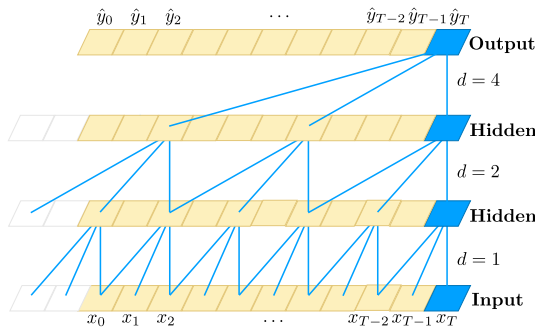

Fig. 7. TCN with dilation factors d = 1; 2; 4 and filter size k = 3 [21]

D. Metric and loss function

To evaluate the performance of developed models a metric is needed. As the networks are used to perform classification instead of regression the accuracy metric is used. This metric calculates how many of the predictions made with the used dataset are correct (e.g. the right RUL range is predicted)
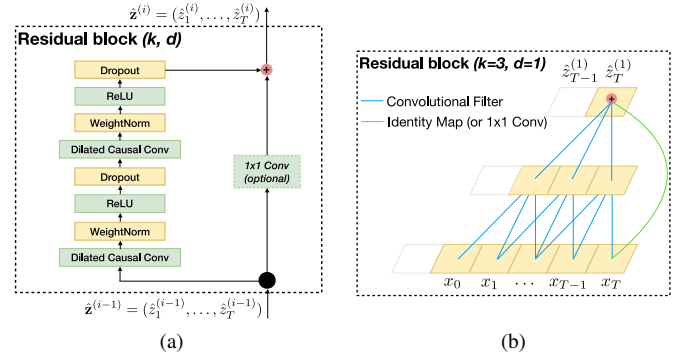

Fig. 8. TCN block elements: (a): Generic TCN block, (b): Example for a TCN block [21]

$$Accuracy = \frac{1}{N} \sum_{i=1}^{N} 1(\hat{y}_i = y_i) \qquad (1)$$

where N is the number of samples with $\hat{y}$ being the prediction and y the target value.

This metric is applied during training and validation to compare different models against each other. The final assessment of the models is made by applying the accuracy metric to the testing dataset.

The used loss function which is used as the objective function for minimization by the backpropagation algorithm is the categorical crossentropy loss function

$$CE = -log(\frac{e^{s_p}}{\sum_{j}^{C} e^{s_j}}) \qquad (2)$$

where s_j is the output of the network for Class j with s_p being the output for the positive class of the sample.

E. Hyperparameter Optimization

To optimize the proposed network architectures a hyperparameter optimization is performed. The hyperparameters include the parameters for the training process (Learning rate, batch size etc.), network parameters (Dropout rate, activation function etc.) and the network architecture itself (number of layers, size of the layers etc.).

There are different strategies for hyperparameter optimization which can be divided in Model-Free and Model-Based approaches. For this study only Model-Free approaches are considered as they are more common and easier to apply. The two typical Model-Free approaches are Grid Search and Random Search [36].

For Grid Search the user defines a discrete number of values for each parameter. The algorithm then tests all possible combinations of these sets of values. This quickly leads to an excessive amount of training runs that need to be done as the number of possible combinations B grows exponentially with the dimensionality d of the search space. If the number of values per parameter is $n = 3$ and the dimensionality is just $d = 5$ the number of combinations already equals $B = n^d = 243$.

Random Search works with a fixed number of evaluations where for each evaluation a value randomly is selected from a predefined set of values for each parameter. The set of values can either be continuous with a lower and upper bound for the values or a discrete set of values. Random Search works better than Grid Search when some parameters are more important than others, which is a property that holds true in many cases [36]. Figure 9 illustrates this property for one important and one unimportant parameter. With a fixed amount of B evaluations Random Search can evaluate up to B different values for each parameter. Whereas Grid Search is limited to $B^{1/N}$ values per parameter. It can be expected that the networks used in this study behave like most networks with regard to the varying importance of the hyperparameters and therefore Random Search is chosen for hyperparameter optimization.
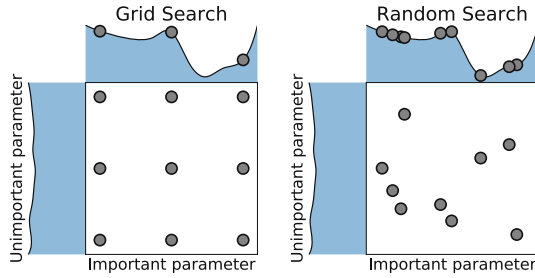

Fig. 9. Comparison of grid search and random search with 9 evaluations on an important and an unimportant parameter [36]

To select the best model after performing the hyperparameter optimization the accuracy of the model on the validation dataset is used.

F. Fine Tuning

After the optimum parameters for a model are found the model can be further improved by running more training epochs. To do so the models are trained with learning rate decay (lrDecay). This approach decreases the learning rate incrementally after a certain number of epochs. In this case the best models from the hyperparameter optimization are taken and trained for a predefined number of epochs on the learning rate which was identified as the best one in the hyperparameter optimization. The learning rate is then lowered before the model is trained again for a fixed number of epochs. This step is repeated until convergence is achieved and no more significant improvements are visible. By using this approach the model in the early stages of training is less likely to get stuck in a local minimum and explores a wider range of possible configurations. As the training comes closer to an optimum the decaying learning rate helps with convergence and avoiding oscillations. According to You et al. [37] there are probably more reasons to the effectiveness of lrDecay besides this common beliefs. The initially large learning rate is, according to them, preventing the network from memorizing noisy data while the decaying learning rate helps with learning complex patterns in the dataset in the later stages of training.

V. RESULTS

A. Model architectures

All RNN architectures are based on the same template. The dataset being normalized before being fed to the models, there is no need for a specific normalization layer. A flexible number of layers is implemented in the networks, as well as a flexible number of cells in each layer which is always a power of 2. A possible dropout and recurrent dropout can also be added to each layer. At the end of the architecture, a dense layer with 20 units is added in order to match the number of RUL classes $C = 20$.

Based on the CNN architecture of Li et al. [9] which was used for aero-engine RUL prediction a 1D-CNN architecture is generated. The first layer of the architecture is for layer normalization. Afterwards a flexible number of 1D-convolutional layers are added which all have the same number of filters and an identical kernel size. The output of the convolutional layers is flattend before being fed into the final dense output layer which has 20 nodes to match the number of RUL classes $C = 20$. As an example Figure 10 shows the final architecture after the hyperparameter optimization with 1000 training structures.
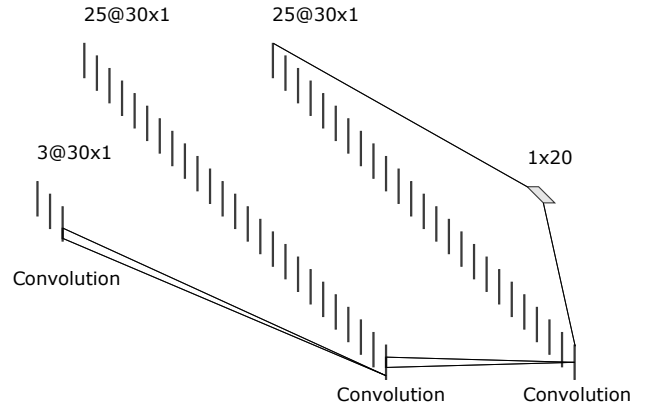

Fig. 10. 1D-CNN architecture after hyperparameter optimization with 1000 training structures

A TCN architecture template is generated based on the results of Liu et al. [10] who used the network for RUL prediction of roller bearings. The architecture consists of multiple TCN residual blocks with the dilation increasing with multiples of 2 for each additional layer. The first layer has a dilation of $d = 1$. Each TCN block features the same number of filters with an identical kernel size. The layer after the TCN blocks is the dense output layer which has 20 nodes to match the number of RUL classes $C = 20$. The skip connection layer is activated for all TCN residual blocks.

B. Hyperparameter optimization

The hyperparameter optimization is performed using Random Search as described in section IV. The used training dataset consists of 100, 500 or 1000 structures. For validation always the same 100 structures different to the training structures are used. The model selection after the optimization is

based on the accuracy of the models on the validation dataset. Not all available parameters of the networks are considered for the optimization as that would increase the computational effort drastically. The reduction also helps to shift the focus of the optimization on the important parameters and avoid varying parameters which have no or only little influence on the accuracy of the network.

1) RNN, LSTM and GRU hyperparameter optimization: Following the same method used for the 1D-CNN and TCN hyperparameter optimization, fixed parameters are set for each architecture, to avoid searching for hyperparameters which are not relevant to the accuracy improvement. Those fixed parameters are the same for the RNN, LSTM and GRU architectures, and can be found in Table II.

TABLE II
FIXED PARAMETERS FOR RNN, LSTM AND GRU HYPERPARAMETER OPTIMIZATION

Parameter	Value
Batch size	4096
Activation function	ReLU
Epochs	500
Sequence length	30

Once those parameters are fixed, useful hyperparameters are identified. These are the ones which can have a significant impact on accuracy improvement. They were identified on 100 structures, and then reused for 500 structures. The optimization on 1000 structures was not done due to a lack of time. The resulting model of the optimization on 500 structures was later used in section V-C1 for the fine tuning on 1000 structures. The found variable hyperparameters are the same for the RNN, LSTM and GRU models. They can be found in Table III.

TABLE III
VARIABLE PARAMETERS FOR RNN, LSTM AND GRU HYPERPARAMETER OPTIMIZATION

Parameter	Value set
Hidden layers	$\{1, 2, 3\}$
Cells per layer	$\{32, 64, 128, 256\}$
Dropout rate	$\{0, 0.1\}$
Recurrent Dropout rate	$\{0, 0.1\}$
Learning rate	$\{10^{-2}, 10^{-3}\}$

The Random Search strategy was then used to optimize those hyperparameters on 100 and 500 structures, with a fixed sliding window size of 30. The learning rate is not listed in the results as the fine tuning will use an adaptative learning rate strategy to optimize the performance of the network. The results of the hyperparameter optimization of the RNNs, LSTMs and GRUs can be found in Table IV.

The results show that RNNs do not need many layers to get a good accuracy compared to CNNs. The best accuracy can be found with no more than 2 or 3 layers in this case. Indeed, too many layers and cells for this amount of data might lead to the model loosing itself, along with the fact that the computational time increases drastically. The Dropout and Recurrent Dropout rates were optimal at 0% meaning that the

TABLE IV
BEST MODELS OF THE RNN, LSTM AND GRU HYPERPARAMETER OPTIMIZATION FOR 100 AND 500 TRAINING STRUCTURES

Training structures	100			500		
Type of architecture	RNN	LSTM	GRU	RNN	LSTM	GRU
Hidden layers	3	2	3	3	2	2
Cells per layer	32	64	256	32	128	256
Dropout rate	0	0	0	0	0	0
Recurrent Dropout rate	0	0	0	0	0	0
Validation accuracy	0.752	0.688	0.726	0.871	0.700	0.814

models did not overfit without dropout for this set of structures. This conclusion is supported by the training history of the model fine tuning shown in Figures 17, 18 and 19 where the validation accuracy follows the training accuracy.

2) 1D-CNN and TCN hyperparameter optimization: Table V lists the fixed parameters of the 1D-CNN optimization. The sliding window length includes multiple values as the influence of that parameter is studied by performing multiple optimization runs with different lengths of the sliding window.

TABLE V
FIXED PARAMETERS FOR 1D-CNN HYPERPARAMETER OPTIMIZATION

Parameter	Value
Batch size	4096
Sliding window length	$\{5, 10, 15, 20, 30, 40\}$
Activation function	ReLU
Padding	Padding with zeros
Dropout	No dropout

Table VI lists the variable parameters and their set of possible values for the CNN hyperparameter optimization. The chosen range for the parameters is the result of a preliminary analysis to identify meaningful boundaries for them.

TABLE VI
VARIABLE PARAMETERS FOR 1D-CNN HYPERPARAMETER OPTIMIZATION

Parameter	Value set
Convolutional layers	$\{2, 4, 6, 8\}$
Filters per layer	$\{15, 20, 25, 30, 35, 40, 45, 50\}$
Kernel size	$\{3, 6, 9, 12\}$
Learning rate	$\{10^{-2}, 10^{-3}\}$

For the 1D-CNN the hyperparameter optimization is performed on 100, 500 and 1000 training structures. For the smallest dataset of 100 structures the optimization is performed on the full range of different sliding window lengths as listed in Table VI. The optimizations on 500 and 1000 structures are only performed with a sliding window size of $N = 30$. All optimization runs are performed with $B = 100$ evaluations for 500 training epochs each.

Figure 11 shows the achieved maximum validation accuracy after the hyperparameter optimization for different lengths of the sliding window. The accuracy increases approximately linearly with size of the sliding window although the absolute value of the improvement remains relatively small. The size of the sliding window can not be increased much above a size of 40 as then the sliding window would be larger than the time

series of some of the structures. A too big sliding window besides that has the disadvantage that it can only be applied if enough data to fill the sliding window is already collected. This means that there could be situations in which the first predictions can only be made just before the part fails or in the worst case after it failed. As a result of these considerations and because of the negligible difference between the sliding window sizes of 30 and 40 a size of $N = 30$ is chosen for all further hyperparameter optimization runs with the 1D-CNN on 500 and 1000 structures.
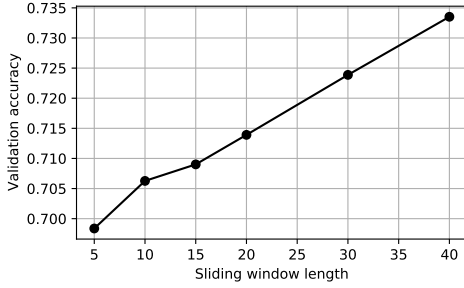

Fig. 11. 1D-CNN hyperparameter optimization for different sliding window sizes for training on 100 structures
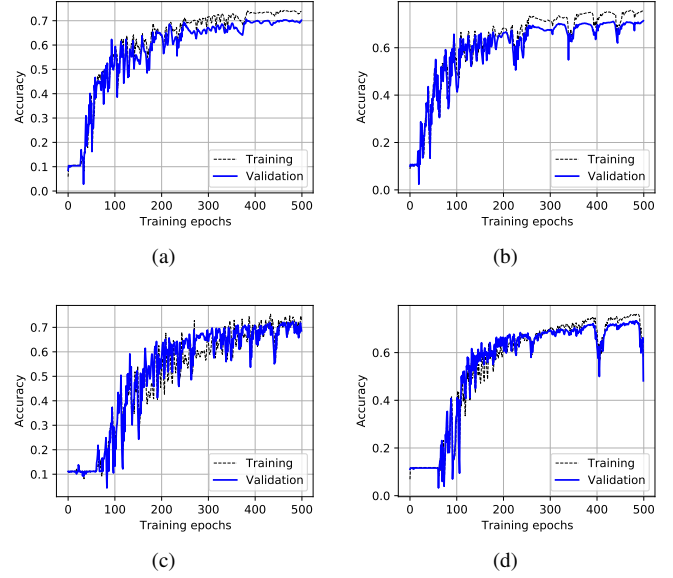

Fig. 12. Training and validation accuracy history for the best models of the 1D-CNN hyperparameter optimization on 100 training structures with a sliding window size of: (a): 10, (b): 20, (c): 30, (d): 40

Table VII shows the different architectures from the hyperparameter optimizations that achieved the best results with the respective sliding window length on 100 training structures. There is no clear trend for the network architecture in relation to the sliding window size. This is backed by the fact that the 2nd and 3rd best networks for each respective hyperparameter optimization can also have significantly different architectures to the best one. This observation leads to the conclusion that there are many different network architectures that can give equal results.

TABLE VII
BEST MODELS OF THE 1D-CNN HYPERPARAMETER OPTIMIZATION ON
100 STRUCTURES FOR DIFFERENT SLIDING WINDOW LENGTHS

Sliding window size	5	10	15	20	30	40
Convolutional layers	4	2	4	2	6	6
Filters per layer	25	35	30	45	20	20
Kernel size	3	6	9	9	6	3
Learning rate	10^{-2}	10^{-2}	10^{-2}	10^{-2}	10^{-2}	10^{-2}
Validation accuracy	0.698	0.706	0.709	0.714	0.724	0.734

Figure 12 shows the history of the training and validation accuracy for the training on 100 structures for some of the different sliding window sizes. There is little to no overfitting on the training dataset for all of the training runs. The 500 training epochs lead to a sufficient convergence of all the runs.

The hyperparameter optimization of the 1D-CNN with 500 training structures and a sliding window size of 30 leads to an improvement of the validation accuracy. Showing that the network architecture if provided with more data can better learn the relationships within the dataset. An increase of the training dataset to 1000 structures leads to no further improvement. This is the result of the lower learning rate of this network which has not fully converged yet (see Figure

13) Table VIII depicts the best network architectures together with the achieved validation accuracy for 100, 500 and 1000 training structures with a sliding window size of 30. There is not clear trend visible in the network architectures indicating that there are many different architectures possible which achieve similar results. This hypothesis is supported by the similar results achieved by some of the other architectures created by the hyperparameter optimizations with distinctly different architectures.

TABLE VIII
BEST MODELS OF THE 1D-CNN HYPERPARAMETER OPTIMIZATION FOR
100, 500 AND 1000 TRAINING STRUCTURES

Training structures	100	500	1000
Sliding window size		30	
Convolutional layers	6	2	4
Filters per layer	20	40	25
Kernel size	6	12	9
Learning rate	10^{-2}	10^{-2}	10^{-3}
Validation accuracy	0.724	0.788	0.789

Figure 13 shows the training history of the best models of the 1D-CNN hyperparameter optimization when training with 500 and 1000 structures respectively. None of the two models shows significant overfitting on the training dataset. Both models are not yet fully converged and therefore have room for improvement. This potential is exploited in the model fine tuning in section V-C2. The training history of the model trained on 500 structures shows an instability at around 480 epochs. Indicating that the learning rate should be reduced which is done in the subsequent model fine tuning.

Table IX lists the fixed parameters of the TCN hyperparameter optimization. The sliding window length includes multiple values as the influence of that parameter is studied by
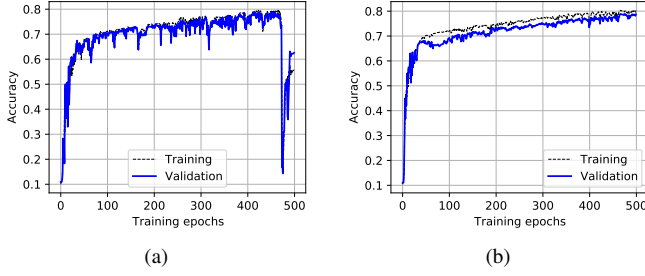
Fig. 13. Training and validation accuracy history for the best models of the 1D-CNN hyperparameter optimization on (a): 500 and (b): 1000 training structures

performing multiple optimization runs with different lengths of the sliding window.

Parameter	Value
Batch size	4096
Sliding window length	$\{10, 15, 20, 30\}$
Activation function	ReLU
Padding	Causal padding
Normalization	Weight normalization

Table X lists the variable parameters and their set of possible values for the TCN hyperparameter optimization. The chosen range for the parameters is the result of a preliminary analysis to identify meaningful boundaries for them. The indicated number of layers directly corresponds the maximal dilation as the dilations rises with multiples of two for each TCN block. For e.g. 4 blocks the dilation in the blocks is $[1, 2, 4, 8]$.

TABLE X
VARIABLE PARAMETERS FOR TCN HYPERPARAMETER OPTIMIZATION

Parameter	Value set
Layers	$\{4, 6, 8, 10\}$
Filters per layer	$\{15, 20, 25, 30, 35, 40, 45, 50\}$
Kernel size	$\{3, 6, 9, 12\}$
Dropout rate	$\{0.0, 0.1, 0.2\}$
Learning rate	$\{10^{-2}, 10^{-3}\}$

As for the 1D-CNN the hyperparameter optimization for the TCN is performed on 100, 500 and 1000 training structures. For the smallest dataset of 100 structures the optimization is performed on the full range of different sliding window lengths as listed in Table X. The optimizations on 500 and 1000 structures are only performed with a sliding window size of $N = 30$. All optimization runs are performed with $B = 50$ evaluations for 500 training epochs each. The number of evaluations is reduced compared to the CNN optimization because of the increased computational effort for the TCNs.

Figure 14 shows the achieved maximum validation accuracy after the hyperparameter optimization for different lengths of the sliding window. There is a significant increase of the accuracy between a length of 15 and 30. The other variations seem to be the result of scatter as a consequence

of neural network training in general as well as the Random Search which leads to different network architectures in each optimization run. To keep a big enough distance to the drop in accuarcy for windows sizes ≤ 20 a sliding window size of $N = 30$ is chosen for all further hyperparameter optimizations with the TCN on 500 and 1000 structures.
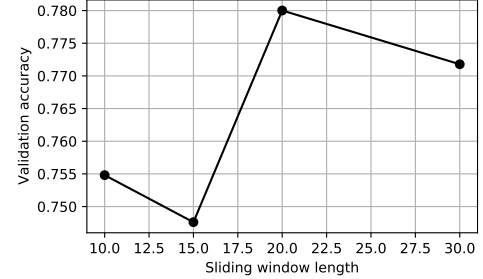

Fig. 14. TCN hyperparameter optimization for different sliding window sizes for training on 100 structures

Table XI shows the different architectures from the hyperparameter optimizations that achieved the best results with the respective sliding window length on 100 training structures. There is a clear trend for the network architecture to have 6 or 8 TCN residual blocks, a kernel size of 2 and no dropout.

TABLE XI
BEST MODELS OF THE TCN HYPERPARAMETER OPTIMIZATION ON 100
STRUCTURES FOR DIFFERENT SLIDING WINDOW LENGTHS

Sliding window size	10	15	20	30
TCN residual blocks	6	8	8	8
Filters per layer	30	45	25	30
Kernel size	2	2	2	2
Dropout rate	0.0	0.0	0.0	0.0
Learning rate	10^{-2}	10^{-2}	10^{-2}	10^{-3}
Validation accuracy	0.755	0.748	0.780	0.771

Figure 12 shows the history of the training and validation accuracy for different sliding window sizes for the training with 100 structures. There is little to no overfitting on the training dataset for all of the training runs. The 500 training epochs lead to a sufficient convergence of all the runs.

Performing the hyperparameter optimization of the TCN with 500 and 1000 structures respectively leads to significant improvements of the validation accuracy. This indicates that the network is able to better learn the relations in the dataset when feed with more data. Table XII depicts the best network architecture together with the achieved validation accuracy for 100, 500 and 1000 training structures with a sliding window size of 30. The resulting architectures are very similar to those depicted in Table XI from the hyperparameter optimization performed on 100 structures with different sliding window sizes. Again featuring 8 TCN residual blocks, a kernel size of 2 and no dropout. Indicating that there is a convergence to an optimal model architecture independent of the used training dataset.

Figure 16 shows the training history of the best models of the TCN hyperparameter optimization when training with
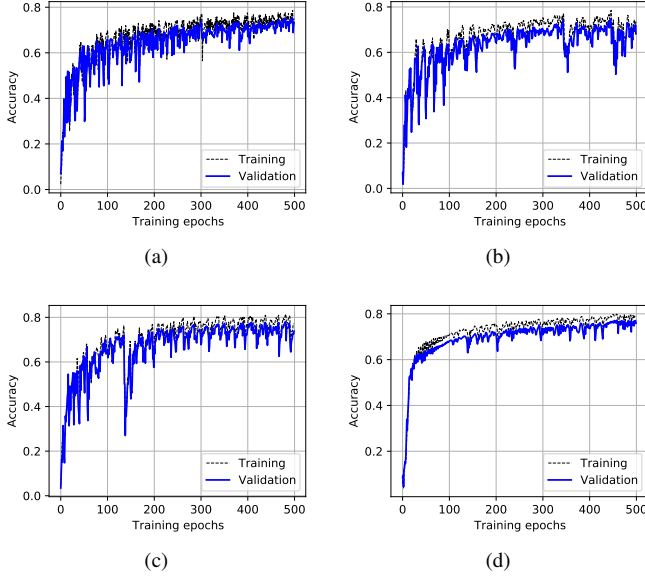
Fig. 15. Training and validation accuracy history for the best model of the TCN hyperparameter optimization on 100 training structures with a sliding window size of: (a): 10, (b): 15, (c): 20, (d): 30

TABLE XII
BEST MODELS OF THE TCN HYPERPARAMETER OPTIMIZATION FOR 100, 500 AND 1000 TRAINING STRUCTURES

Training structures	100	500	1000
Sliding window size		30	
TCN residual blocks	8	8	8
Filters per layer	30	25	35
Kernel size	2	2	2
Dropout rate	0.0	0.0	0.0
Learning rate	10^{-3}	10^{-2}	10^{-2}
Validation accuracy	0.772	0.883	0.908

500 and 1000 structures respectively. None of the two models shows a sign of overfitting on the training dataset. Both models are not yet fully converged and therefore have room for improvement. This potential is exploited in the model fine tuning in section V-C2. Both training histories show instabilities during draining, indicating that the learning rate should be reduced which is done in the subsequent model fine tuning.
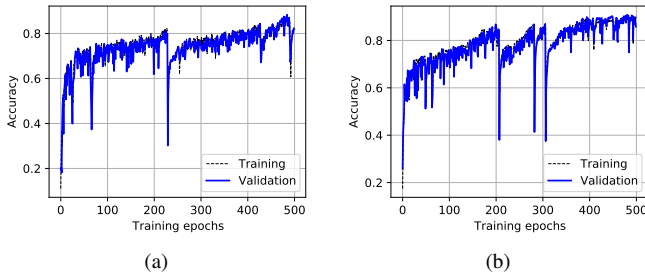

Fig. 16. Training and validation accuracy history for the best models of the TCN hyperparameter optimization on (a): 500 and (b): 1000 training structures

C. Fine Tuning

As the hyperparameters are optimized, the resulting models are trained with an adaptive learning rate (lrDecay) to optimize their performance. The models are further refined on the same dataset on which the optimization was performed. lrDecay starts with a learning rate of 10^{-2} or 10^{-3} depending on which value was chosen in the hyperparameter optimization, decreasing to 10^{-3}, 10^{-4} and then 10^{-5}. With each learning rate, the models were trained for 500 epochs which leads to maximum of 2000 training epochs. After the fine tuning the models are tested on the testing dataset to evaluate their final performance.

1) RNN, LSTM and GRU fine tuning: For the RNN, LSTM and GRU models the results of the training history can be found grouped by the number of structures in Figures 17, 18 and 19. It can be clearly observed that the lrDecay strategy allows a better training for each model. Once the models are trained, they are evaluated on the testing dataset. All the results for the validation and testing accuracy can be found in Table XIII.
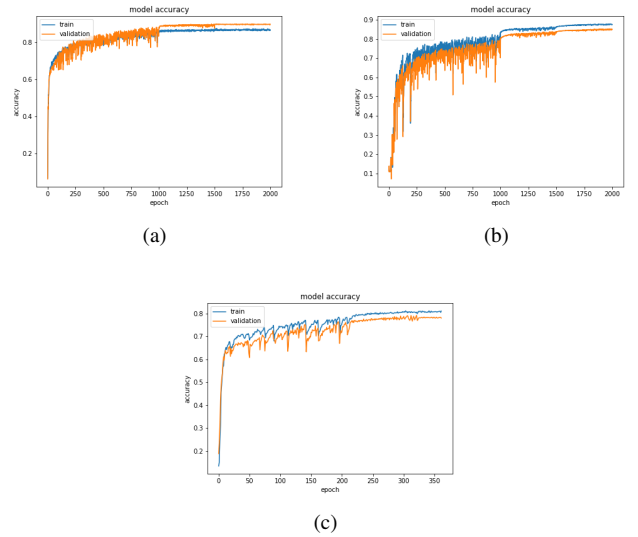

Fig. 17. Training and validation accuracy history for 100 training structures with lrDecay: (a): RNN, (b): LSTM, (c): GRU

Little to no overfitting can be observed in each training. In addition, some training historys show an unstable improvement, with even a decreasing accuracy after some learning rate changes. This could have an impact on the final accuracy. Nevertheless, it seems that decreasing the learning rate improves the stability of the training.

Regarding the final validation and testing accuracies, there is a significant difference between 100 and 500 training structures. The different models increased both their validation and testing accuracies, even though the differences between 500 and 1000 structures are less notable. The highest improvement is noticed with the GRU model, reaching 97% validation accuracy with 1000 training structures.
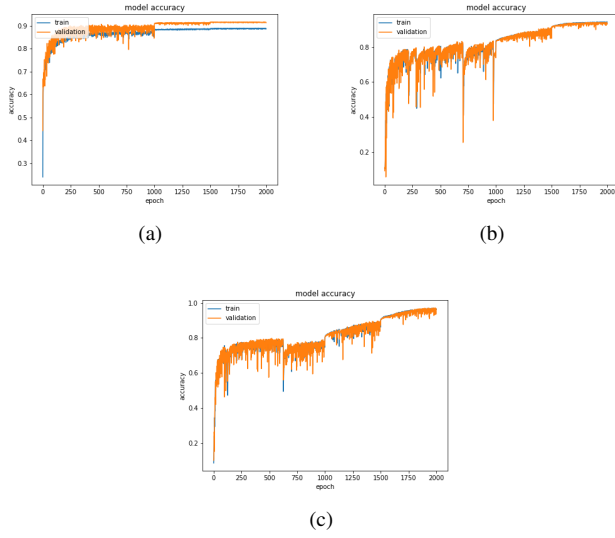
Fig. 18. Training and validation accuracy history for 500 training structures with lrDecay: (a): RNN, (b): LSTM, (c): GRU
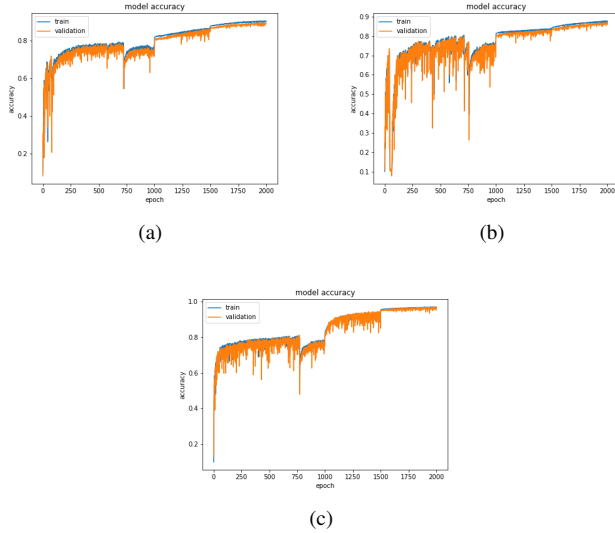

Fig. 19. Training and validation accuracy history for 1000 training structures with lrDecay: (a): RNN, (b): LSTM, (c): GRU

However, a huge difference is observed between the validation and the testing accuracy. This could be due to the accuracy metric used. As the boundaries for the classification follow a parabolic equation, the first classes are narrower than the last classes. Studying the distribution of the different RUL classes to predict in the testing dataset in the training dataset might show that they are less present in the training dataset. This makes it more difficult to predict these classes in the testing dataset. A possible solution might be to choose another metric which would take into account this uneven distribution of the RUL classes.

2) 1D-CNN and TCN fine tuning: For each of the best identified network architectures of the 1D-CNN and TCN

hyperparameter optimizations further training with lrDecay is performed to improve their performance. Out of the models which were optimized on 100 structures the models with a sliding window size of 30 are chosen for further refinement.

Figure 20 depicts the training histories for the fine tuning on 100, 500 and 1000 structures. The networks show little to no overfitting on the training dataset. There is steady improvement of the accuracy towards convergence except for the training on 500 structures which shows a steep drop of the accuracy at around 500 epochs.
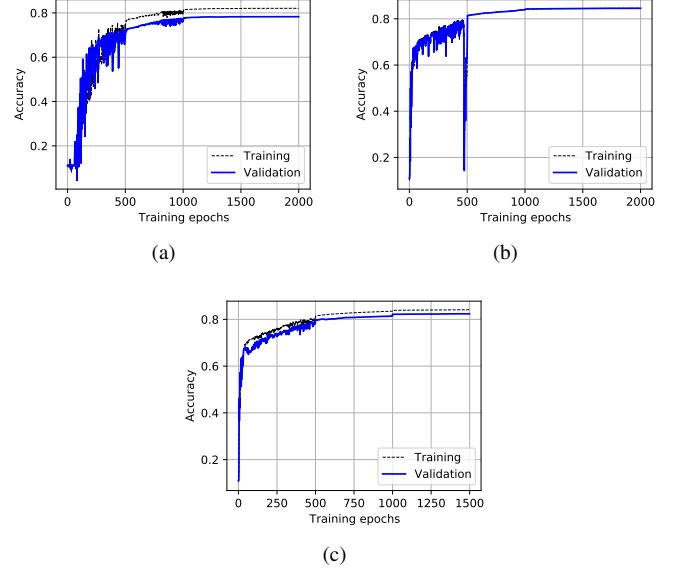

Fig. 20. Training and validation accuracy history for the best models of the 1D-CNN hyperparameter optimization on (a): 100, (b): 500 and (c): 1000 structures after fine tuning the models with lrDecay on the same datasets

The training histories of the TCN fine tuning can be seen in Figure 21. The best model from the hyperparameter optimization on 1000 structures was not only fine tuned on 1000 structures but also on the full dataset of 9900 structures to see if any improvements can be realized when using much more training data (see Figure 21 (d)). During the first phase of training with the highest learning rate there are strong oscillations of the accuracy for all the models. The first decrease of the learning rate helps to stabilize the training and for all the models gives a significant rise to the accuracy. In the later stages of the training all the models show a stable convergence. Only the model trained on 100 structures shows a bit of overfitting on the training dataset while the other models show no such signs.

3) Model comparison: As a final validation all the fine tuned models are tested with the testing dataset of 100 structures. Table XIII shows an overview of the achieved accuracy for all RNN (RNN, LSTM and GRU) and CNN models (1D-CNN and TCN).

It can be noticed that for RNN models, the difference between the validation accuracy and the testing accuracy is notable. The networks have difficulties to generalize the
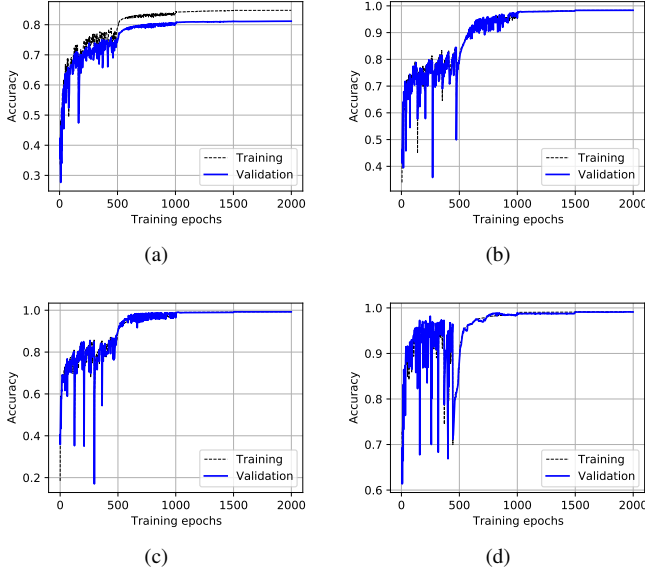
Fig. 21. Training and validation accuracy history for the best models of the TCN hyperparameter optimization on (a): 100, (b): 500, (c): 1000 and (d): 9900 structures after fine tuning the models with lrDecay on the same datasets

Training structures	100		500		1000		9 900	
Accuracy	Val	Test	Val	Test	Val	Test	Val	Test
RNN	**0.90**	**0.84**	0.91	0.90	0.89	0.78	—	—
LSTM	0.85	0.73	0.93	0.83	0.93	0.72	—	—
GRU	0.78	0.70	0.96	0.77	0.97	0.75	—	—
1D-CNN	0.78	0.82	0.84	0.84	0.82	0.84	—	—
TCN	0.81	0.82	**0.98**	**0.98**	**0.99**	**0.99**	**0.99**	**1.00**

of the models. The best performance in general was achieved by TCN models. Confirming the good results with TCNs of other researchers like Bai et al. [21] and Li et al. [9]. This result again questions the general practice to use RNN models as the first choice for time series prediction while CNN models should be used for image classification and related tasks. The TCN models when trained on more than 500 structures achieved closed to 100% accuracy confirming their excellent suitability to time series prediction problems.

The RNN models, especially the GRUs, achieved good performances on the validation dataset while when tested on the testing dataset there is a significant drop in performance. This might be the result of the testing dataset being focused on short RUL values close to failure of the plates. In this area there are many different RUL classes because of the parabolic distribution of the class boundaries. The GRUs seem to have troubles generalizing to this area while they might work very well on the classes with bigger RUL values. Thus, a lead to explore would be a hybrid model combining a GRU and TCN architecture, to improve learning of the different patterns in the data.

The in general good results achieved on this dataset should come at no surprise as the dataset is synthetic without the flaws of real world data. There is no noise in the data which would never be the case in reality. The virtual strain gauges are always placed at the exact same location on the plates while in reality there is always a position tolerance when placing them on a structure. The synthetic dataset can also provide the models with amounts of data which are not available in reality. Especially the amount of data available until the End of life (EOL) of the structures.

Fur further research it is important to train and test the models on noisy data and focus on improving their accuracy when trained on smaller datasets, e.g. on 100 structures. These smaller datasets should also include less data towards the EOL of the structures.

Right now the models are restricted to a fixed sliding window size. They therefore can not use less but also not more of the available data than dictated by the sliding window size. A possible solution to consider for this problem would be to use a much larger sliding window together with zero padding when not enough data to fill the window is available. This way the networks could use all of the available past and current data independently of the sliding window size and the length of the currently available time series of the structure.

patterns learned to new sets of data. But, as previously analysed in section V-C1, this could also be the result of the RUL classification which gives a larger bandwidth to the last classes and therefore leads to an imbalance of the training dataset towards the classes with higher RUL values. The testing dataset meanwhile focuses on the first classes, which are smaller. This imbalance leads to an increasing possibility of wrong predictions of the RUL on the testing dataset. One lead to explore would be to adapt the accuracy metric to take into account this imbalance of the training and testing data. Nonetheless, GRUs seem to work better on large datasets, reaching 97% validation accuracy when trained on 1000 structures.

For the 1D-CNN and TCN models there is a steady increase in the achieved accuracy on the testing dataset if the amount of structures for training is increased. The increase in testing accuracy corresponds largely to the increase in validation accuracy. The testing accuracy is in the same order of magnitude as the validation accuracy indicating that the networks generalize well to new sets of data. In general TCNs work better than 1D-CNNs, especially on the larger datasets of 500 and 1000 structures where the TCNs achieve close to 100% accuracy. When trained on the complete dataset of 9900 training structures the TCN achieved 100% accuracy on the testing dataset.

VI. CONCLUSIONS AND OUTLOOK

The aim of this study to predict the RUL of pre cracked plates based on strain gauges data with Deep Learning methods could be achieved. All investigated models were successfully trained on the available dataset and achieved an accuracy of at least 70% on the testing dataset. It usually was the case that more available training data lead to a better performance

REFERENCES

[1] Y. LeCun, Y. Bengio, and G. Hinton, "Deep learning," *Nature*, vol. 521, no. 7553, pp. 436–444, 2015, ISSN: 1476-4687. DOI: 10.1038/nature14539.

[2] J. Z. Sikorska, M. Hodkiewicz, and L. Ma, "Prognostic modelling options for remaining useful life estimation by industry," *Mechanical Systems and Signal Processing*, vol. 25, no. 5, pp. 1803–1836, 2011, ISSN: 0888-3270. DOI: 10.1016/j.ymssp.2010.11.018. [Online]. Available: https://www.sciencedirect.com/science/article/pii/S0888327010004218.

[3] A. Voulodimos, N. Doulamis, G. Bebis, and T. Stathaki, "Recent developments in deep learning for engineering applications," *Computational Intelligence and Neuroscience*, vol. 2018, p. 8141259, 2018, ISSN: 1687-5265. DOI: 10.1155/2018/8141259.

[4] J. J. Montero Jimenez, S. Schwartz, R. Vingerhoeds, B. Grabot, and M. Salaün, "Towards multi-model approaches to predictive maintenance: A systematic literature survey on diagnostics and prognostics," *Journal of Manufacturing Systems*, vol. 56, pp. 539–557, 2020, ISSN: 0278-6125. DOI: 10.1016/j.jmsy.2020.07.008. [Online]. Available: https://www.sciencedirect.com/science/article/pii/S0278612520301187.

[5] S. Wu, K. L. Tsui, N. Chen, Q. Zhou, Y. Hai, and W. Wang, "Prognostics and health management: A review on data driven approaches," *Mathematical Problems in Engineering*, vol. 2015, p. 793161, 2015, ISSN: 1024-123X. DOI: 10.1155/2015/793161.

[6] A. Akrim, C. Gogua, R. Vingerhoeds, and M. Salaun, "Review of prognostics approaches with a particularfocus on the current machine learning algorithms," 2021.

[7] E. Zio, "Prognostics and Health Management of Industrial Equipment," in *Diagnostics and Prognostics of Engineering Systems: Methods and Techniques*, S. Kadry, Ed., ISBN13: 9781466620957, IGI Global, Sep. 2012, pp. 333–356. DOI: 10.4018/978-1-4666-2095-7.ch017. [Online]. Available: https://hal-supelec.archives-ouvertes.fr/hal-00778377.

[8] L. Xu, S. F. Yuan, J. Chen, and Q. Bao, "Deep learning based fatigue crack diagnosis of aircraft structures," in *7th Asia-Pacific Workshop on Structural Health Monitoring*, 2018. [Online]. Available: https://www.ndt.net/search/docs.php3?id=24093.

[9] X. Li, Q. Ding, and J.-Q. Sun, "Remaining useful life estimation in prognostics using deep convolution neural networks," *Reliability Engineering & System Safety*, vol. 172, pp. 1–11, 2018, ISSN: 0951-8320. DOI: 10.1016/j.ress.2017.11.021. [Online]. Available: https://www.sciencedirect.com/science/article/pii/S0951832017307779.

[10] C. Liu, L. Zhang, and C. Wu, "Direct remaining useful life prediction for rolling bearing using temporal convolutional networks," (Dec. 6, 2019), Xiamen, China: IEEE, Dec. 6, 2019, pp. 2965–2971, ISBN: 978-1-7281-2486-5. DOI: 10.1109/SSCI44817.2019.9003163.

[11] M. Yuan, Y. Wu, and L. Lin, "Fault diagnosis and remaining useful life estimation of aero engine using lstm neural network," in *2016 IEEE International Conference on Aircraft Utility Systems (AUS)*, 2016, pp. 135–140. DOI: 10.1109/AUS.2016.7748035.

[12] Y. Wu, M. Yuan, S. Dong, L. Lin, and Y. Liu, "Remaining useful life estimation of engineered systems using vanilla lstm neural networks," *Neurocomputing*, vol. 275, pp. 167–179, 2018, ISSN: 0925-2312. DOI: 10.1016/j.neucom.2017.05.063. [Online]. Available: https://www.sciencedirect.com/science/article/pii/S0925231217309505.

[13] K. Park, Y. Choi, W. Choi, H.-Y. Ryu, and H. Kim, "Lstm-based battery remaining useful life prediction with multi-channel charging profiles," *IEEE Access*, vol. PP, pp. 1–1, Jan. 2020. DOI: 10.1109/ACCESS.2020.2968939.

[14] W. A. Little, "The existence of persistent states in the brain," in *From High-Temperature Superconductivity to Microminiature Refrigeration*, B. Cabrera, H. Gutfreund, and V. Kresin, Eds. Boston, MA: Springer US, 1996, pp. 145–164, ISBN: 978-1-4613-0411-1. DOI: 10.1007/978-1-4613-0411-1_12.

[15] J. J. Hopfield, "Neural networks and physical systems with emergent collective computational abilities," *Proceedings of the National Academy of Sciences*, vol. 79, no. 8, pp. 2554–2558, 1982, ISSN: 0027-8424. DOI: 10.1073/pnas.79.8.2554. eprint: https://www.pnas.org/content/79/8/2554.full.pdf. [Online]. Available: https://www.pnas.org/content/79/8/2554.

[16] Y. Lecun, L. Bottou, Y. Bengio, and P. Haffner, "Gradient-based learning applied to document recognition," *Proceedings of the IEEE*, vol. 86, no. 11, pp. 2278–2324, 1998. DOI: 10.1109/5.726791.

[17] J. L. Elman, "Finding structure in time," *Cognitive Science*, vol. 14, no. 2, pp. 179–211, 1990, ISSN: 0364-0213. DOI: 10.1016/0364-0213(90)90002-E. [Online]. Available: https://www.sciencedirect.com/science/article/pii/036402139090002E.

[18] M. I. Jordan, "Chapter 25 - serial order: A parallel distributed processing approach," in *Neural-Network Models of Cognition*, ser. Advances in Psychology, J. W. Donahoe and V. Packard Dorsel, Eds., vol. 121, North-Holland, 1997, pp. 471–495. DOI: 10.1016/S0166-4115(97)80111-2. [Online]. Available: https://www.sciencedirect.com/science/article/pii/S0166411597801112.

[19] J. Yan and P. Wang, "Blade material fatigue assessment using elman neural networks," vol. 2007, Jan. 2007. DOI: 10.1115/IMECE2007-43311.

[20] S. E. Kramti, J. Ben Ali, L. Saidi, M. Sayadi, and E. Bechhoefer, "Direct wind turbine drivetrain prognosis approach using elman neural network," in *2018 5th International Conference on Control, Decision and*

Information Technologies (CoDIT), 2018, pp. 859–864. DOI: 10.1109/CoDIT.2018.8394926.

[21] S. Bai, J. Z. Kolter, and V. Koltun, "An empirical evaluation of generic convolutional and recurrent networks for sequence modeling," *CoRR*, vol. abs/1803.01271, 2018. arXiv: 1803.01271. [Online]. Available: http://arxiv.org/abs/1803.01271.

[22] A. Saxena, K. Goebel, D. Simon, and N. Eklund, "Damage propagation modeling for aircraft engine run-to-failure simulation," in *2008 International Conference on Prognostics and Health Management*, 2008, pp. 1–9. DOI: 10.1109/PHM.2008.4711414.

[23] O. Fink, Q. Wang, M. Svensén, P. Dersin, W.-J. Lee, and M. Ducoffe, "Potential, challenges and future directions for deep learning in prognostics and health management applications," *Engineering Applications of Artificial Intelligence*, vol. 92, p. 103 678, 2020, ISSN: 0952-1976. DOI: 10.1016/j.engappai.2020.103678. [Online]. Available: https://www.sciencedirect.com/science/article/pii/S0952197620301184.

[24] T. Tinga and R. Loendersloot, "Physical model-based prognostics and health monitoring to enable predictive maintenance," in *Predictive Maintenance in Dynamic Systems: Advanced Methods, Decision Support Tools and Real-World Applications*, E. Lughofer and M. Sayed-Mouchaweh, Eds. Cham: Springer International Publishing, 2019, pp. 313–353, ISBN: 978-3-030-05645-2. DOI: 10.1007/978-3-030-05645-2_11.

[25] F. Timothy, M. Devinder, and H. Iain, "F-35 joint strike fighter structural prognosis and health management an overview," Jan. 2009. DOI: 10.1007/978-90-481-2746-7_68.

[26] A. Akrim, "Description algorithm."

[27] P. Paris and F. Erdogan, "A critical analysis of crack propagation laws," *Journal of Basic Engineering*, vol. 85, no. 4, pp. 528–533, Dec. 1963. DOI: 10.1115/1.3656900.

[28] C.-L. Liu, W.-H. Hsaio, and Y.-C. Tu, "Time series classification with multivariate convolutional neural network," *IEEE Transactions on Industrial Electronics*, vol. 66, no. 6, pp. 4788–4797, Dec. 6, 2019. DOI: 10.1109/TIE.2018.2864702.

[29] W. Xiao, "A probabilistic machine learning approach to detect industrial plant faults," Mar. 2016. arXiv: 1603.05770 [stat.ML].

[30] G. Chen, "Recurrent neural networks (rnns) learn the constitutive law of viscoelasticity," *Computational Mechanics*, vol. 67, Mar. 2021. DOI: 10.1007/s00466-021-01981-y.

[31] Y. Bengio, P. Simard, and P. Frasconi, "Learning long-term dependencies with gradient descent is difficult.," eng, *IEEE transactions on neural networks*, vol. 5, pp. 157–66, 2 1994. DOI: 10.1109/72.279181.

[32] S. Hochreiter and J. Schmidhuber, "Long Short-Term Memory," *Neural Computation*, vol. 9, no. 8, pp. 1735–1780, Nov. 1997, ISSN: 0899-7667. DOI: 10.1162/neco.1997.9.8.1735. eprint: https://direct.mit.edu/neco/article-pdf/9/8/1735/813796/neco.1997.9.8.1735.pdf.

[33] Y. Wu, M. Schuster, Z. Chen, *et al.*, "Google's neural machine translation system: Bridging the gap between human and machine translation," Sep. 2016. arXiv: 1609.08144 [cs.CL].

[34] R. Rana, "Gated recurrent unit (gru) for emotion classification from noisy speech," Dec. 2016. arXiv: 1612.07778 [cs.HC].

[35] R. A. Sayyad, "How to use convolutional neural networks for time series classification," *Medium*, [Online]. Available: https://medium.com/@Rehan_Sayyad/how-to-use-convolutional-neural-networks-for-time-series-classification-80575131a474.

[36] M. Feurer and F. Hutter, "Hyperparameter optimization," in *Automated Machine Learning*, Springer, Cham, 2019, pp. 3–33.

[37] K. You, M. Long, J. Wang, and M. I. Jordan, *How does learning rate decay help modern neural networks?* 2019. arXiv: 1908.01878 [cs.LG].